2013 IEEE/RSJ International Conference on
Intelligent Robots and Systems (IROS)
November 3-7, 2013. Tokyo, Japan

Towards Snake-like Soft Robots: Design of Fluidic Fiber-Reinforced Elastomeric Helical Manipulators

Joshua Bishop-Moser and Sridhar Kota

Abstract*— Tendril helical motions and snake robots have a multitude of potential applications from climbing to anchoring to complex manipulation in fields such as medical, gas/oil energy, and manufacturing. Constructing a snake robot from a fluid driven, fiber reinforced elastomeric enclosure (FREE), complex helical motions are created in a lightweight, low cost, simple structure. The snake-like manipulators are created by forming a hollow cylindrical elastomer that is reinforced with two families of fibers and one additional fiber. The manipulator is then driven by changing the volume of fluid contained within, thus forming the desired helical patterns. The design of this continuum structure is analyzed for all possible fiber angles and the FREE radius. The parameters of the resulting helix including pitch and radius are determined analytically, without the need for finite element methods. Three prototypes at different points in the design space are fabricated and tested to verify the analytical model.

I. INTRODUCTION

Continuum elastic structures are utilized in both nature and engineered solutions, as they provide adaptability to the environment, complex shapes and motion patterns, and the ability to merge structure and actuation functions. The addition of fluids to these elastic structures can again be seen in nature from octopus tentacles to round worms [1]. These structures work by using the contained fluid to transmit and redirect the forces and displacements via the fluid pressure. The structure surrounding the fluid is a fiber-reinforced elastomeric enclosure (FREE), which we have previously investigated for one and two families of fibers [2] [3] [4]. Hirai et al. previously performed a preliminary analysis of deformable reinforced elastomeric cylinders [5], which are a small subset of the full range of FREE structures that we discovered. FREEs use the fluid in pure compression and the fibers in pure tension to provide a compliant mechanism for transmitting the fluid pressure to desired output motions. The advantages of using FREEs are that they are lightweight, low cost, and are very high power density force transducers. These attributes have been advantageously used in McKibben actuators, which employ symmetrical helical fibers to produce only axial force and motion. McKibben actuators represent another small subset of FREEs we discovered, and have been extensivly studied by Chou et al. [6], Tsagarakis et al. [7], Tondu et al. [8], and many others. McKibben actuators have been used in many robotic applications described in review papers by Trivedi et al. [9] and Webster et al. [10].

Joshua Bishop-Moser is a Graduate Student in the Department of Mechanical Engineering, University of Michigan, Ann Arbor, MI 48109, USA joshbm@umich.edu
Sridhar Kota is a Professor of Mechanical Engineering, University of Michigan, Ann Arbor, MI 48109, USA kota@umich.edu

This paper investigates the creation of helical, or snake-like, shapes using FREEs. Snake robots have advantages in grasping with distributed force, traversing narrow regions, climbing, and many other actions. These actions lead to applications in pipe inspection, mobile robots, medical devices, and a range of other useful areas. The challenge for snake robots is often the weight, complexity, energy usage, and cost to create numerous actuated segments in series. Ample applications do not need the full range of motions, rather many of the multitudes of motions can be reduced to a primary single actuated degree of freedom in a helical spiral pattern or in bending. Using FREEs offers the ability to create these elaborate single degree of freedom shapes without using a multitude of joints or actuators, instead using fluid pressure and fiber reinforced elastomer enclosing the fluid. This paper explores the use of FREEs with two families of fibers and an additional single fiber to create manipulators with this elaborate single degree of freedom, towards eventually creating full mobile robots.

There have been a substantial number of studies on snake robots; many are captured in a review by Hirose et al. [11]. Takayama and Hirose demonstrated some applications and advantages of a helical snake motion for locomotion and manipulation, and they addressed the fabrication of a fluid driven snake [12]. The resulting design, however, was segmented, complex, heavy, and not continuum. Suzumori presents multi-segment manipulators with limited helical motion capabilities [13]. Tanaka presents an underconstrained fiber-reinforced pneumatic snake design [14]. There have been other fluid driven cylindrical manipulators that are only able to obtain bending. Our previous work on FREEs only considered families of fibers, with many closely packed fibers of the same angle making up a family. The inclusion of a single additional fiber to the existing FREE configurations containing two families of fibers alters the deformation patterns and assumptions previously used. This produces either pure bending or in most cases a helical pattern. The analytical equations of the kinematics that drive this motion are determined and the design space is mapped.

II. FREE: GOVERNING BEHAVIOR

In our previous papers we described cylindrical fiber-reinforced elastomeric enclosures (FREEs) that have two families of fibers. A family of fibers is a parallel set of fibers that are closely packed and aligned at the same angle as each other. When two families of fibers are wrapped around a cylindrical volume, the volume enclosed is directly correlated with the motion at the end of the cylinder. The angles of the fibers are described using the fiber helix angles α and β with respect to the axial direction. A diagram illustrating a cylinder with two families of fibers and the corresponding fiber angles is shown in Figure 1. These structures are capable of producing axial elongation and contraction, clockwise and counter-clockwise rotation, and screw motions that are coordinated axial and rotational motions. The motion that the FREE will produce depends on the helix angles, α and β.

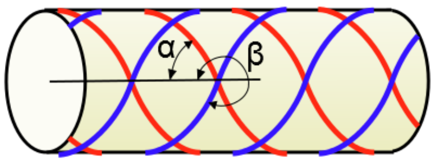

Fig. 1. Fiber-reinforced elastomeric enclosure (FREE) with 2 families of helical fibers at angles α and β. β can also be written as $(\beta - 360°)$. In this example α is approximately $45°$ and β is $-45°$.

This study expands our prior work by adding a single fiber to the existing FREE structure. The existing FREE was fully constrained to one degree of actuation for nearly all α and β combinations. All of the existing FREE configurations other than those with axial fibers have a degree of freedom in bending. The addition of the single fiber will consequently utilize this degree of freedom and cause a controlled bending when pressurized. The rotation of the FREE from the two families of fibers and the angle of the added single fiber, referred to as γ, will cause the bending direction to spiral around the FREE. The resulting shape of this new manipulator will be a helical pattern. Pure bending is still possible, as that is simply a spiral with a helix angle of zero.

The scope of this study encompasses cylindrical fiber-reinforced elastomeric enclosures (FREEs) that have two families of fibers and a single additional fiber. As described above, these fibers can all be described using the fiber helix angles α, β, and γ with respect to the axial direction. Figure 2 (a) shows the helical fiber angle notation for an unactuated FREE with 2 families of fibers and a single fiber. Axial fibers have an α of $0°$, circumferential are $90°$, and the spirals are $-90° < \alpha < 0°$ and $0° < \alpha < 90°$. Angles that are $90° < \alpha < 270°$ can be written as $(\alpha - 180°)$ and angles that are $270° \leq \alpha < 360°$ can be written as $(\alpha - 360°)$. This allows all fiber to be described using the $-90° \leq \alpha \leq 90°$ notation.

The deformation behavior of FREEs are governed by the inextensibility of fibers and incompressibility of fluid. Some simplifying assumptions about the FREE's geometry and deformation behavior restrict the analysis and conclusions to a certain class of cylindrical FREEs. These are:

1) Initial and final cross-sections are circular.
2) The fibers are infinitely small and closely laid with large volume fractions.
3) Fluid pressure is evenly distributed.
4) The effect of the elastomer that encloses the fluid is ignored. The elastomer has zero stiffness effect on the fiber motion and infinite stiffness against bulging between fibers.
5) The deformed FREE has fiber angles averaged across each cross-section.
6) All analysis is quasi-static.

The axial and radial deformation of a cylinder are expressed as stretch ratios λ_1 and λ_2 respectively. The single fiber causes bending, with the radius of curvature of the bend expressed as ρ. An actuated FREE is shown in Figure 2 (b), with λ_1 shown along the axial length, l, and λ_2 along the FREE radius, r. θ is the number of rotations (in radians) that a fiber will make while spiraling the length of an unactuated FREE, while θ^* is the number of rotations for a deformed FREE. δ is the rotation of one end of a FREE relative to the other due to the change in volume from the unactuated state (again in radians). This value can also be seen as the additional rotation of the fibers from the unactuated to actuated state. V^* is the volume enclosed in the FREE after the volume change. κ is the inverse of ρ ($\kappa = \frac{1}{\rho}$). With these definitions in place, Section II-A will describe the equations we have previously found for two families of fibers in Eqs.1-5; the new equations derived from adding the additional single fiber are presented in the remaining equations.

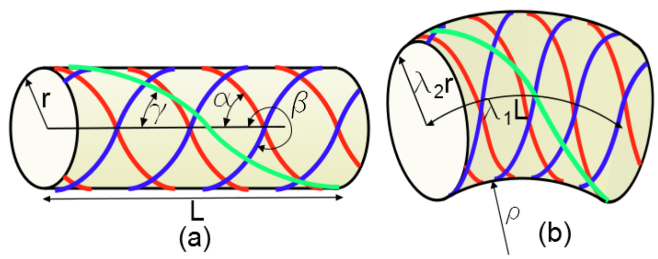

Fig. 2. (a) Fiber-reinforced elastomeric enclosure (FREE) with 2 families of helical fibers at angles α and β and a single helical fiber at angle γ. (b) Pressurized FREE with stretch ratios λ_1 and λ_2 and bend radius ρ.

A. Kinematic Equations

Our previous work [4] determined five important equations that describe the deformation of FREEs. Eq. 1 is the equation describing the inextensibility of a fiber. λ_1, λ_2, α, and the ratio $\frac{\theta^*}{\theta}$ must hold the relationship shown in Eq. 1 such that the fiber does not extend. Eq. 2 is the equation describing the volume after deformation. This shows that the volume is found from the stretch ratios and the unactuated volume (unactuated volume $V = \pi r^2 l$). Eq. 3 shows the equation for the number of rotations that a fiber will make spiraling the length of an unactuated FREE. Eq. 4 shows how λ_2 (the radial expansion) is a function of the angles α and β and the axial expansion λ_1. Eq. 5 shows how δ (the rotation caused by actuation) is a function of α, β, and λ_1, as well as the length and radius of the manipulator. These equations are necessary for derivation and understanding of the kinematics of the snake manipulator that is formed when the single fiber is added.

$$\lambda_1^2(\cos(\alpha))^2 + \lambda_2^2(\sin(\alpha))^2(\frac{\theta^*}{\theta})^2 = 1 \quad (1)$$

$$V^* = \lambda_2^2\lambda_1\pi r^2 l \quad (2)$$

$$\theta = \frac{tan(\alpha)l}{r} \quad (3)$$

$$\lambda_2 = \frac{\frac{\alpha}{|\alpha|}\, C_\beta\sqrt{1 - C_\alpha^2\lambda_1^2} - \frac{\beta}{|\beta|}\, C_\alpha\sqrt{1 - C_\beta^2\lambda_1^2}}{S_{\alpha-\beta}} \quad (4)$$

$$\delta = \frac{l}{r}\,\frac{\frac{\beta}{|\beta|}\, S_\alpha\sqrt{1 - \lambda_1^2\, C_\beta^2} - \frac{\alpha}{|\alpha|}\, S_\beta\sqrt{1 - \lambda_1^2\, C_\alpha^2}}{\frac{\alpha}{|\alpha|}\, C_\beta\sqrt{1 - \lambda_1^2\, C_\alpha^2} - \frac{\beta}{|\beta|}\, C_\alpha\sqrt{1 - \lambda_1^2\, C_\beta^2}} \quad (5)$$

$$where:\ S_x = \sin(x),\, C_x = \cos(x)$$

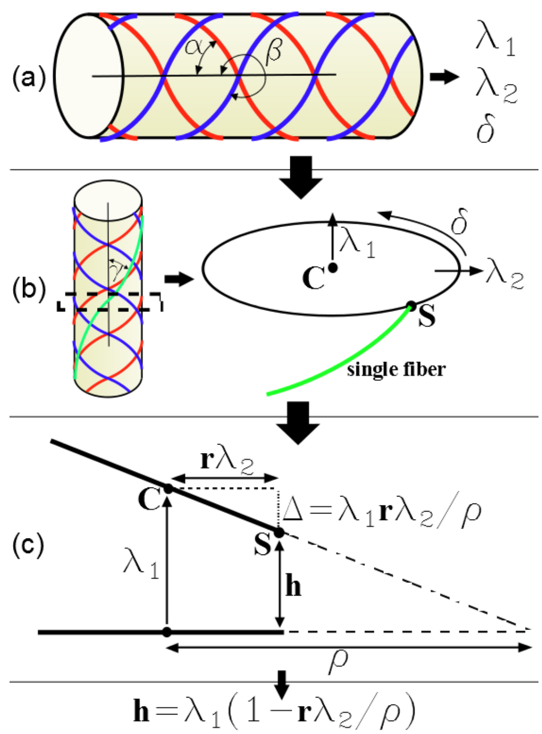

Fig. 3. Derivation of the effect of a single fiber on bend radius ρ (a) The two families of the fibers of the fiber-reinforced elastomeric enclosure (FREE) determine stretch ratios λ_1, λ_2, and rotation δ. (b) The resulting free body diagram of a small section when a single fiber is applied to the two family FREE. (c) Diagram of a length normalized section of the FREE, showing the relationship between ρ and change in displacement in the axial direction.

As described previously, the addition of the single fiber causes a FREE with two families of fibers to bend due to the additional constraint imposed by the single fiber. Since this is a single fiber, rather than a family of fibers, the equation for the inextensibility of the fiber will be different from the one shown in Eq. 1 due to the FREE's ability to bend toward the fiber constraint. Figure 3 shows how the axial extension component of the fiber length constraint is modified when there is a single fiber added. The two families of FREEs will determine λ_1, λ_2, and δ, seen in Figure 3 (a). The addition of the single fiber will interact at a single point, shown in Figure 3 (b) as point "S". λ_1, λ_2, and δ combine with the bend radius (ρ), as shown in Figure 3 (c), to determine the length normalized axial extension at the single fiber. Equation 6 is the fiber inextensibility equation for the single fiber. It is derived in the same manner as Eq. 1, by setting the length before and after deformation to be equal. Equation 7 is Eq. 6 rewritten with ρ as the dependent variable, and α, β, γ, λ_1, λ_2, and δ as the independent variables. Equation 8 further refines ρ to an expression that is only dependent on the parameters of α and β, and the operational variable of λ_1. This simplification is done using the equations for λ_2 and δ (Eqs. 4 and 5 respectively). Equation 9 shows curvature, κ, which is the inverse of ρ. With these equations in place, it is now understood how α and β will affect the relationship between axial expansion and bending.

$$\lambda_1^2(1 - \frac{r\lambda_2}{\rho})^2(\cos(\gamma))^2 + \lambda_2^2(\sin(\gamma))^2(\frac{\theta^*}{\theta})^2 = 1 \quad (6)$$

$$\rho = \frac{r\lambda_1\lambda_2}{\lambda_1 - \sqrt{\sec(\gamma)^2 - \lambda_2^2\tan(\gamma)^2(\tan(\gamma) + \frac{r\delta}{l})^2}} \quad (7)$$

$$\rho = \frac{r\lambda_1 X}{S_{\alpha-\beta}\,\lambda_1 - \sqrt{(S_{\alpha-\beta}\,\sec(\gamma))^2 - T_\gamma^2(T_\gamma\, X + W)^2}} \quad (8)$$

$$\kappa = \frac{S_{\alpha-\beta}\,\lambda_1 - \sqrt{(S_{\alpha-\beta}\,\sec(\gamma))^2 - T_\gamma^2(T_\gamma\, X + W)^2}}{r\lambda_1 X} \quad (9)$$

$$where:$$

$$X = \frac{\alpha}{|\alpha|}\, C_\beta\sqrt{1 - \lambda_1^2\, C_\alpha^2} - \frac{\beta}{|\beta|}\, C_\alpha\sqrt{1 - \lambda_1^2\, C_\beta^2}$$

$$W = \frac{\beta}{|\beta|}\, S_\alpha\sqrt{1 - \lambda_1^2\, C_\beta^2} - \frac{\alpha}{|\alpha|}\, S_\beta\sqrt{1 - \lambda_1^2\, C_\alpha^2}$$

$$S_x = \sin(x),\, C_x = \cos(x),\, T_x = \tan(x)$$

The relationship between the expansion and the volume contained is determined, as the controlled variable is volume, not λ_1. Eq. 10 shows λ_1 as a function of λ_2, which is derived by rewriting Eq. 4. Equation 11 is an implicit function defining the relationship between λ_1 and the volume of the FREE. This is derived by substituting the value of λ_2 into Eq. 10. λ_2 is found by rewriting Eq. 2 as $\lambda_2^2 = \frac{V}{\lambda_1\pi r l}$. Equation 11 can be solved explicitly for λ_1 as a function of volume, and the resulting equation is too long to display in this paper. The explicit form of Eq. 11 can be substituted into Eq. 8 to derive ρ as a function of volume; the resulting equation is again too large to display in this paper.

$$\lambda_1 = \frac{\sqrt{2\lambda_2^2(C_\alpha^2 + C_\beta^2) - S_{\alpha+\beta}^2 - \lambda_2^4\, S_{\alpha-\beta}^2}}{2\, C_\alpha\, C_\beta\lambda_2} \quad (10)$$

$$-\frac{4V\cos(\beta)^2\cos(\alpha)^2}{\pi r^2 l}\lambda_1^3 - \sin(\alpha+\beta)^2\lambda_1^2 + ...$$
$$\frac{2V(\cos(\alpha)^2 + \cos(\beta)^2)}{\pi r^2 l}\lambda_1 - \frac{V^2\,\sin(\alpha-\beta)^2}{\pi^2 r^4 l^2} = 0 \quad (11)$$

The deformed shape of the FREE is a helix, and the two key parameters of the helix for many applications are the helix angle, ϕ, and the helix radius, R. Equation 12 defines ϕ in terms of the rotation caused by the two families of fibers (δ), the number of rotations of the single fiber (θ), the bend radius (ρ), and the axial length of the FREE (l). Equation

13 defines R using these same variables. Equation 14 shows how θ is derived, and is the same form as Eq. 3. Equation 15 shows ϕ as a function of parameters α, β, and γ and variable λ_1. ϕ can be further modified to be a function of α, β, and γ and the control variable, volume, by substituting in Eq. 11 and Eq. 8 into Eq. 15. The detailed equation for R is computed in a similar manner, but these equations are too large to display in this paper.

$$\phi = \arctan(\frac{\delta_{eff}}{l\kappa}) = \arctan(\frac{(\delta+\theta)\rho}{l}) \quad (12)$$

$$R = \frac{\rho}{1+(\frac{\delta_{eff}}{l\kappa})^2} = \frac{\rho}{1+(\frac{(\delta+\theta)\rho}{l})^2} \quad (13)$$

$$\theta = \frac{tan(\gamma)l}{r} \quad (14)$$

$$\phi = atan(\frac{\lambda_1(W+XT_\alpha)}{\lambda_1 - \sqrt{\sec(\gamma)^2 - \lambda_2^2\tan(\gamma)^2(\tan(\gamma)+\frac{r\delta}{l})^2}}) \quad (15)$$

$$where:$$

$$X = \frac{\alpha}{|\alpha|}C_\beta\sqrt{1-\lambda_1^2C_\alpha^2} - \frac{\beta}{|\beta|}C_\alpha\sqrt{1-\lambda_1^2C_\beta^2}$$

$$W = \frac{\beta}{|\beta|}S_\alpha\sqrt{1-\lambda_1^2C_\beta^2} - \frac{\alpha}{|\alpha|}S_\beta\sqrt{1-\lambda_1^2C_\alpha^2}$$

$$S_x = \sin(x),\ C_x = \cos(x),\ T_x = \tan(x)$$

III. Design Space

There are three main design variables of the snake continuum robots: α, β, and γ, and one operational variable of normalized volume (normalized to the unactuated volume). The axial length of the FREE does not affect the helix angle or helix radius. Radius of the FREE does not affect the helix angle and is linearly proportional to the helix radius. Material and geometric properties determine stiffness, which likely have some effect on the motion, but are outside the scope of this study, per the simplifying assumptions. While it is difficult to simultaneously visualize the effect of four independent variables on the output values, plots have been created to illustrate various sections of the design space.

Figure 4 explores how the helix angle, ϕ, is effected by the parameters α and β and the operational variable of volume. This is done by fixing the remaining variable, γ, at a value of 10°. The volume is set at five different volumes, and α and β are plotted over their entire range. The plot shows α and β on the X and Y axes and the resulting ϕ on the Z axis. This is done for the five different volumes, shown in different colors. Figure 5 explores how the helix radius, R, depends on the same independent variables (α, β, and volume). The helix radius has been normalized for FREE radius in the plot. The single fiber angle, γ, is set at 7°.

Figures 4 and 5 show the wide range of helix angles and radii that are possible, even without changing the angle of the single fiber. With an increased volume, the helix angle in Figure 4 ranges from $\frac{\pi}{2}$ to $\frac{-\pi}{2}$ depending only on the angles of the families of fibers. Some regions, such as those seen for α and β both greater than zero will have a helix angle that is highly sensitive to volume, while other regions with have minimal sensitivity. The helix radius exhibits similar properties with the α and β both greater than zero regions showing high sensitivity to volume changes. The dependence on volume is highly non-linear, with some regions expanding in helix radius, and then contracting as the volume is increased.

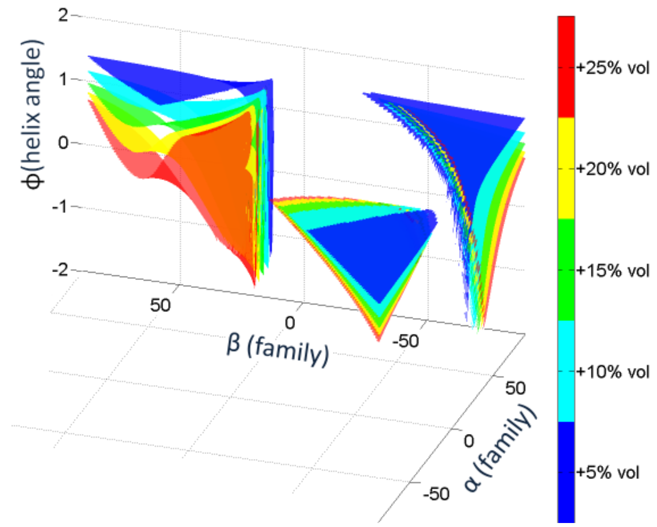

Fig. 4. The effect of percent volume increase and fiber angles α and β (in degrees) on the device's helix angle, ϕ (in radians). The single fiber, γ, is set at 10°, and the radius of the device is set at 0.2. Five volume change values: +5%, +10%, +15%, +20%, and +25% are set and the resulting ϕ as a function of α and β is plotted.

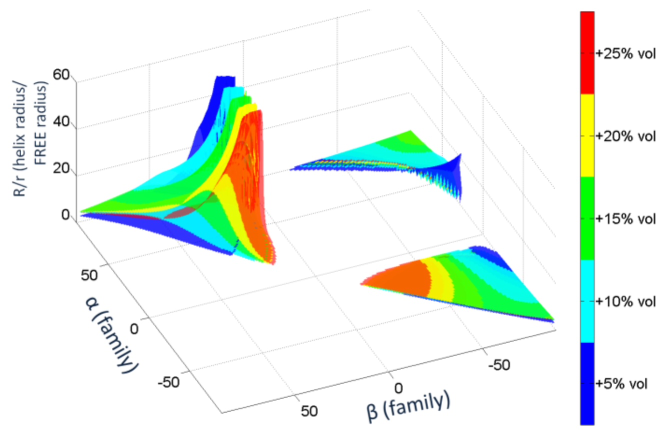

Fig. 5. The effect of percent volume increase and fiber angles α and β (in degrees) on the device's helix radius (relative to the radius of the FREE), R/r (normalized radius). The single fiber, γ, is set at 7°, and the radius of the device is set at 0.2. Five volume change values: +5%, +10%, +15%, +20%, and +25% are set and the resulting R/r as a function of α and β is plotted. Plot clipped above at 50.

Figure 6 illustrates the effects of the fiber angles β and γ on ϕ. To do this, α (one of the two families of fibers) is fixed at 65 degrees and volume increase is fixed at 10%. The resulting contour plot shows the values of ϕ over β on the X axis and γ on the Y axis. The large range of possible ϕ values, even with both α and volume fixed can be seen in the plot. The sensitivity of the snake configuration to changes in fiber angle can also be readily understood. Small errors are seen in the region with β between 0° and 5°, as the single fiber passes through the axial configuration.

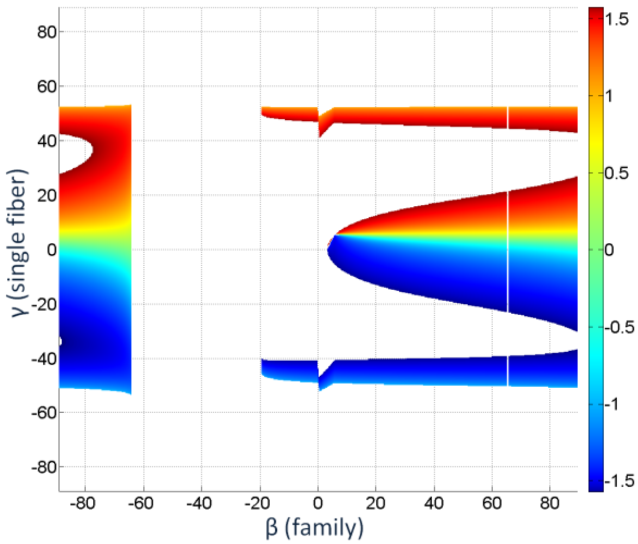

Fig. 6. Helix angle, ϕ, across fiber angles β and γ (in degrees). One of the families of fibers, α, is set at 65°, volume change is set at +10%, and the radius of the device is set at 0.2.

IV. Experimental Validation

To verify the accuracy of the model in predicting the kinematics of the snake-like manipulators, multiple prototypes were fabricated and analyzed. These prototypes were constructed across a diverse selection of α, β, and γ. The helix radius was determined through measurement, while the helix angle was determined by combining this radius with the pitch of the helix. The first prototype snake tested has dimensions $\alpha = -70°$, $\beta = -30°$, and $\gamma = 1°$. The snake prototype has a FREE radius of 5.5 mm and was inflated to a volume increase of 35% ($\frac{V_{final}}{V_{initial}} = 1.35$). The analytical models predict this configuration and inflation to have a snake helix angle of 73.1°, and coil with a radius of 4.46 mm. The resulting snake is shown in Figure 7. The measured snake helix angle of the prototype is 59.4°. The radius is 9.3 mm. The helix angle has an error of 18.7%.

Fig. 7. Snake with $\alpha = -70°$, $\beta = -30°$, and $\gamma = 1°$. The snake prototype has a body radius of 5.5 mm and was inflated to a volume increase of 35%. The image is the inflated snake (image rotated 90 degrees, gravity going right).

The second prototype has dimensions $\alpha = 88°$, $\beta = -60°$, $\gamma = 10°$, FREE radius of 5.5 mm, and was inflated to a volume increase of 30%. The analytical models predict this configuration and inflation to have a snake helix angle of 60.94°, and coil with a radius of 5.74 mm. The resulting snake is shown in Figure 8. The measured snake helix angle of the prototype is 55.7°. The radius is 11.43 mm. The helix angle has an error of 8.6%.

The third prototype snake tested has dimensions $\alpha = 65°$, $\beta = -80°$, and $\gamma = 5°$, FREE radius of 5.5 mm, and was inflated to a volume increase of 15%. The analytical models predict this configuration and inflation to have a snake helix angle of 8.13°, and coil with a radius of 31.9 mm. The resulting snake is shown in Figure 9. The measured snake helix angle of the prototype is 9.1°. The radius is 50.8 mm. The helix radius has an error of 11.9% or 0.97°.

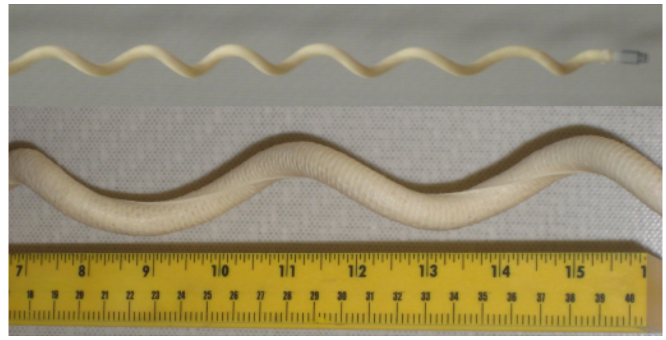

Fig. 8. Snake with $\alpha = 88°$, $\beta = -60°$, and $\gamma = 10°$. The snake prototype has a body radius of 5.5 mm and was inflated to a volume increase of 30%. Top image is the full snake (image rotated 90 degrees, gravity going right), and the bottom image compares the snake to a measuring device.

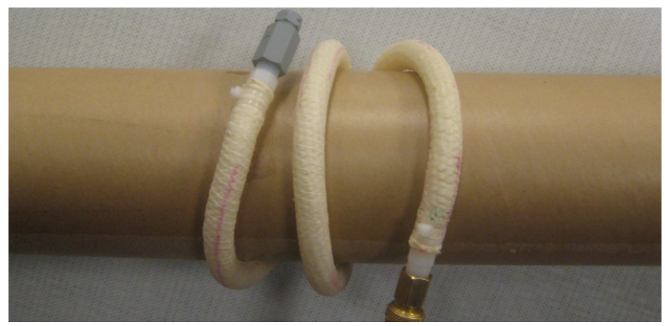

Fig. 9. Snake with $\alpha = 65°$, $\beta = -80°$, and $\gamma = 5°$. The snake prototype has a body radius of 5.5 mm and was inflated to a volume increase of 15%. The image is the inflated snake (image rotated 90 degrees, gravity going right).

These dimensions are highly sensitive to manufacturing and material assumptions, such as inextensibility of the fibers and exact fiber angles, thus providing opportunities for deviations from values derived from the model. While the helix angles matched rather closely, the helix radius had larger errors. This is likely caused by the single fiber not having an infinite stiffness as the model assumes, thus allowing axial extension without bending. This would result in a larger helix radius than the predicted one, which is seen in all three prototypes.

V. Conclusions

This paper illustrated a kinematics approach to determining the deformation pattern of continuum snake-like helical manipulators that use volume increase in a fiber reinforced elastomeric enclosure (FREE). The motion of the snake mechanism was solved as a function of the contained volume for any given fiber angle α, β, and γ, as well as for FREE radius. Visual representations of portions of the design space are shown, and three test cases were fabricated and actuated to show their fit with the analytical model. The primary contributions of this paper are

1) Determination of the kinematic deformation patterns for FREEs with two families of fibers and an additional single fiber.
2) Creation of simple equations that can be used to both analyze and synthesize snake like pneumatic manipulators.
3) Enabling applications that were previously inaccessible due to a lack of lightweight, simple, low cost, high power density snake robots.

One possible application is distributed force grasping, seen in Figure 10. These snakes can grasp and hold weights that are at least 100 times their own weight. With grasping, climbing will be a clear next step for the technology. The snakes can also grasp the inside of a pipe when inflated, thus opening up pipe inspection, anchoring, and various medical applications. This pipe anchoring can be seen in Figure 11. The helical motion can also be used for manipulation in complex environments, with numerous manufacturing, medical, and inspection based applications. Many of these applications require a lightweight, high power density snake, with simplicity and low cost being additional benefits. Nearly all of the applications will require an understanding of how the design parameters of α, β, γ, and FREE radius, as well as the operational parameter of volume affect the deformation patterns.

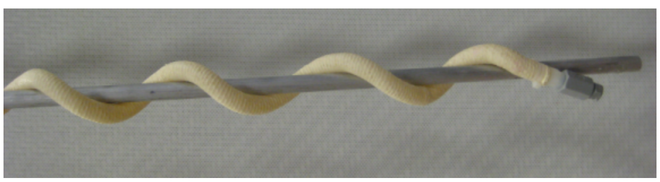

Fig. 10. Snake with $\alpha = 88°$, $\beta = -60°$, and $\gamma = 10°$ grasping a metal rod. The snake can hold 100s of times its weight in this grasping motion.

Fig. 11. Snake anchoring to the inside of a clear tube using the kinematics of its body deformation under volumetric expansion.

A. Future Work

The model presented was able to capture the motion characteristics of the verification prototypes, yet there was still a residual error. Future work will refine the model in two key ways to more accurately predict the deformation. The first refinement is to add a material model. The simplifying assumption removed any consideration of material to allow for an easy analytical solution, rather than a computational finite element based one. This will have the added benefit of allowing the snakes to be pressure controlled, rather than volume controlled, as the material stiffness will link the pressure to the volume. The second refinement is to consider the change in the fiber angles of the two families of fibers as the snake deforms. The model currently assumes that the deformation is small enough to not substantially change the fiber angle of the families of fibers (α and β), using a linear model of their deformation. Additionally, as the snake bends due to the single fiber, the change in fiber angle of the families of fibers due to this bend is not considered. Both of these assumptions are made to form a simple analytical function that can quickly map a large design space (computing approximately 100,000 helix angles and snake radius values per second on a desktop computer in Matlab). A full non-linear model would, however, likely increase the accuracy of the results. The other main areas for future work are to combine these actuators in parallel and focus on practical applications.

VI. Acknowledgements

The authors would like to acknowledge the assistance of Darlene Yao and Dr. Girish Krishnan. This work was supported by the National Science Foundation under NSF Award 1030887 and the Graduate Research Fellowship.

References

[1] S. Vogel, Comparative Biomechanics. Princeton, New Jersey: Princeton, 2003.
[2] J. Bishop-Moser, G. Krishnan, C. Kim, and S. Kota, 'Design of Soft Robotic Actuators Using Fluid-filled Fiber-reinforced Elastomeric Enclosures in Parallel Combinations,' *Intelligent Robots and Systems (IROS), 2012 IEEE/RSJ International Conference on*, vol., no., pp.4264,4269, 7-12 Oct. 2012.
[3] J. Bishop-Moser, G. Krishnan, C. Kim, and S. Kota, 'Kinematic Synthesis of Fiber Reinforced Soft Actuators in Parallel Combination,' *Proceedings of the 36th Mechanisms and Robotics Conference at ASME IDETC 2012*, Chicago, IL, August 2012.
[4] G. Krishnan, J. Bishop-Moser, C. Kim, and S. Kota, 'Evaluating Mobility Behavior of Fluid Filled Fiber- Reinforced Elastomeric Enclosures,' *Proceedings of the 36th Mechanisms and Robotics Conference at ASME IDETC 2012*, Chicago, IL, August 2012.
[5] S. Hirai, P. Cusin, H. Tanigawa, T. Masui, S. Konishi, and S. Kawamura, 'Qualitative Synthesis of Deformable Cylindrical Actuators Through Constraint Topology,' *The Proc. of IEEE Int. Conf. on Intelligent Robots and Systems*, Vol. 1, pp. 197 - 201, 2000.
[6] C.-P. Chou and B. Hannaford, 'Measurement and modeling of McKibben pneumatic artificial muscles,' Robotics and Automation, IEEE Transactions on , vol.12, no.1, pp.90,102, Feb 1996.
[7] N. Tsagarakis and D.G. Caldwell, 'Improved modelling and assessment of pneumatic muscle actuators,' Robotics and Automation, 2000. Proceedings. ICRA '00. IEEE International Conference on , vol.4, no., pp.3641,3646 vol.4, 2000.
[8] B.Tondu and P.Lopez, 'Modeling and control of McKibben artificial muscle robot actuators,' Control Systems, IEEE , vol.20, no.2, pp.15,38, Apr 2000.
[9] D. Trivedi, C. Rahn, W. Kierb, and I. Walker, 'Soft Robotics: Biological Inspiration, State of the Art, and Future Research,' *Applied Bionics and Biomechanics*, Vol. 5, No. 3, pp. 99 - 117, Sept. 2008.
[10] R. J. Webster III, and B. Jones, 'Design and Kinematic Modeling of Constant Curvature Continuum Robots: A Review,' *Int. J. of Robotics Research*, Vol. 29, No. 13, pp. 1161 - 83, Nov. 2010.
[11] S. Hirose, H. Yamada, 'Snake-like Robots: Machine Design of Biologically Inspired Robots,' *IEEE Robotics and Automation Magazine*, v 16, n 1, p 88-98, 2009.
[12] T. Takayama, S. Hirose, 'Amphibious 3D Active Cord Mechanism "HELIX" With Helical Swimming Motion,' *IEEE International Conference on Intelligent Robots and Systems*, v 1, p 775-780, 2002.
[13] K. Suzumori, 'Elastic Materials Producing Compliant Robots,' *Robotics and Autonomous Systems*, Volume 18, Issues 12, July 1996, Pages 135-140
[14] Y. Tanaka, 'Study of Artificial Rubber Muscle,' *Mechatronics* Vol. 3. No. 1. pp. 59-75. 190 1992.